Prediction of Ideal Topological Semimetals with Triply Degenerate Points in the NaCu_{3}Te_{2} Family

Jianfeng Wang, Xuelei Sui, Wujun Shi, Jinbo Pan, Shengbai Zhang, Feng Liu, Su-Huai Wei, Qimin Yan, and Bing Huang

Prediction of Ideal Topological Semimetals with Triply Degenerate Points in NaCu$_3$Te$_2$ Family

Jianfeng Wang[1], Xuelei Sui[2,1], Wujun Shi[2], Jinbo Pan[3], Shengbai Zhang[4,1], Feng Liu[5,6*], Su-Huai Wei[1], Qimin Yan[3†] and Bing Huang[1‡]

[1] *Beijing Computational Science Research Center, Beijing 100193, China*

[2] *Department of Physics and State Key Laboratory of Low-Dimensional Quantum Physics, Tsinghua University, Beijing 100084, China*

[3] *Department of Physics, Temple University, Philadelphia, PA 19122, USA*

[4] *Department of Physics, Applied Physics, and Astronomy, Rensselaer Polytechnic Institute, Troy, New York 12180, USA*

[5] *Department of Materials Science and Engineering, University of Utah, Salt Lake City, Utah 84112, USA and*

[6] *Collaborative Innovation Center of Quantum Matter, Beijing 100084, China*

Abstract

Triply degenerate points (TDPs) in band structure of a crystal can generate novel TDP fermions without high-energy counterparts. Although identifying ideal TDP semimetals, which host clean TDP fermions around the Fermi level (E_F) without coexisting of other quasiparticles, is critical to explore the intrinsic properties of this new fermion, it is still a big challenge and has not been achieved up to now. Here, we disclose an effective approach to search for ideal TDP semimetals via selective band crossing between antibonding s and bonding p orbitals along a line in the momentum space with C_{3v} symmetry. Applying this approach, we have successfully identified the NaCu$_3$Te$_2$ family of compounds to be ideal TDP semimetals, where two and only two pairs of TDPs are located around the E_F. Moreover, we demonstrate a fundamental mechanism to modulate energy splitting between a pair of TDPs, and illustrate the intrinsic features of TDP Fermi arcs in these ideal TDP semimetals.

* Email: fliu@eng.utah.edu
† Email: qiminyan@temple.edu
‡ Email: Bing.Huang@csrc.ac.cn

0

As topological phase extends from insulators [1, 2] to semimetals [3–6], new quasiparticles analogous to elementary particles in high-energy physics emerge in these topological materials, such as Weyl (Dirac) fermions in Weyl (Dirac) semimetals [7–10]. Interestingly, the band theory has shown that the crystal symmetries in solids allow for the existence of other types of topological quasiparticle excitations even without high-energy counterparts [11], which can be hosted by three-, six-, or eight-fold degenerate points in the band structures [12]. Especially, the triply degenerate points (TDPs) [13–21], formed by the crossing of a double-degenerate band and a nondegenerate band, can be recognized as an intermediate phase between Weyl (double-degenerate) and Dirac (fourfold-degenerate) fermions. The TDP semimetals have been predicted to have some unique properties, e.g., Lifshitz transitions of Fermi surface [15, 16], helical anomaly [16], large nonsaturating or negative magnetoresistance [22], and unconventional quantum Hall effects [23].

Generally speaking, the TDPs can appear along the high-symmetry lines with the C_{3v} symmetry group in the Brillouin zone (BZ), because it allows for both one- (1D) and two-dimensional (2D) double-group representations. For example, the tensile-strained HgTe [13], CuPt-ordered $InAs_{0.5}Sb_{0.5}$ [14], WC-type or half-Heusler compounds [15–21] have been suggested as host candidates. Also, several experimental measurements have been carried out to reveal the electronic structures around TDPs in the MoP and WC compounds [24–26]. However, one of the key problems for exploring the intrinsic properties of TDP fermions is the lack of ideal TDP semimetals, in which the TDPs around the Fermi level (E_{F}) do not coexist with other quasiparticle bands. Therefore, it is of great importance to search for ideal host materials having only TDP fermions around E_{F}.

In this Letter, we disclose an effective approach to realize clean TDPs near the E_{F} via selective band crossing between antibonding s (s^*) and bonding p orbitals along the line with C_{3v} symmetry. Importantly, we have successfully identified that the $NaCu_3Te_2$ family of compounds are ideal TDP semimetals. Moreover, a simple mechanism has been revealed to control the energy splitting between the two adjacent TDP nodes. Finally, we illustrate the unique features of Fermi arc of TDP fermion, in comparison with 2- and 4-component fermions.

One of the most common characters found in previous TDP candidates is that the TDPs are mainly induced by different d bands crossing near the Fermi level [15–19], e.g., crossing of $d_{x^2-y^2,xy}$-d_{z^2} bands, as shown in Fig. 1(a). Because of the high degeneracy (5 orbitals)

and localized nature (narrow band widths) of d orbitals, these d bands usually cross each other around E_F multiple times in the entire BZ. As a result, besides the TDPs, other types of quasiparticle bands appear also around E_F [15, 17–19], which unfortunately overshadows the TDPs. Comparing with d bands, s and p bands have low degeneracy (1 or 3 orbitals) and delocalized dispersion (wide band widths), which may play a useful role in creating clean TDPs. Here, we propose that the band inversion between antibonding s^* orbital of cation at the conduction band minimum (CBM) and bonding p orbitals of anion at the valence band maximum (VBM) in a compound may achieve clean sp-band TDPs, as illustrated in Fig. 1(a). When s^* and p bands cross each other along the C_{3v} symmetric line in BZ, the s^* bands will be double-degenerate ($J_z = \pm 1/2$) and $p_{x,y}$ bands will split into two nondegenerate bands ($J_z = \pm 3/2$) due to spin-orbit coupling (SOC) effect in a non-centrosymmetric structure. Belonging to different group representations, the hybridization between s^* and $p_{x,y}$ orbitals is forbidden by symmetry, so that the s^*-p band inversion will produce two pairs of desirable TDPs. Interestingly, in spite of the existence of s^*-p band inversion in HgTe [13] and half-Heusler compounds [21], the higher symmetry of p bands (Γ_8) at the Γ point leads to multiple degenerated states coexisting with the TDPs that are resulted from the p-p band crossing around E_F. Thus, the key to our approach is to find those compounds with the desired s^*-p ($p_{x,y}$ here) band inversion in the whole BZ.

For a typical semiconducting compound with the s^* orbital at the CBM and p orbital at the VBM, their band energies can be determined from a two-level tight-binding model of the s-s coupling and p-p coupling between cation and anion, respectively [27]: $E_{\text{CBM}} = (\varepsilon_s^c + \varepsilon_s^a)/2 + \{[(\varepsilon_s^c - \varepsilon_s^a)/2]^2 + V_{ss}^2\}^{1/2}$, $E_{\text{VBM}} = (\varepsilon_p^c + \varepsilon_p^a)/2 - \{[(\varepsilon_p^c - \varepsilon_p^a)/2]^2 + V_{pp}^2\}^{1/2}$. The ε_s^c and ε_s^a, ε_p^c and ε_p^a are the cation and anion s and p atomic orbital energies, respectively, and V_{ss} and V_{pp} are the coupling potentials for s and p states, respectively. First, to get band inversion between the s^*- and p-orbital bands, a simple way is to find a material with close energies between E_{CBM} and E_{VBM}. Considering the suitable values of ε_s^c and ε_p^a, together with the typical strengths of V_{ss} and V_{pp} [27], we can confine our search in compounds with cation and anion candidates listed in Fig. 1(b). Besides the s-s and p-p couplings, other orbital hybridizations may also affect the energies of the s and p bands, which are compound dependent [28]. Second, to acquire both 1D and 2D double group representations for the TDPs, our search is further confined into those compounds with the C_{3v} subgroup. Following these rules, we have successfully identified that $NaCu_3Te_2$ is the targeted TDP semimetal
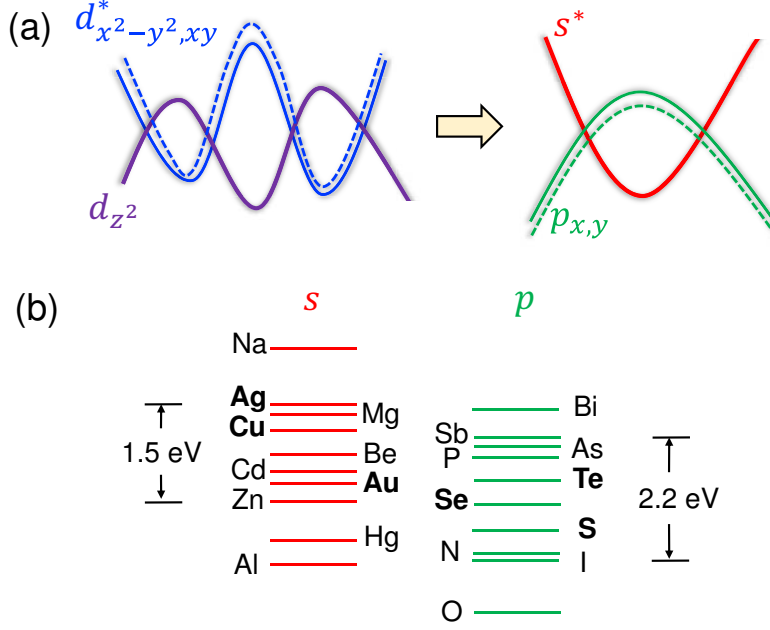
2

FIG. 1: (a) Schematic plot of d^*-d TDP semimetals and our strategy for s^*-p TDP semimetals. Double-degenerate bands are drawn as thick solid lines, whereas nondegenerate bands are drawn as thin solid or dashed lines. (b) Atomic s and p orbital energy levels of targeted cations and anions considered in our study.

[29].

As shown in Fig. 2(a), $NaCu_3Te_2$ (ICSD No.: 60860) has a non-centrosymmetric rhombohedral structure with space group $R3m$ (No. 160). The fully relaxed lattice constant for its 18-atom conventional cell is $a = b = 4.25$ Å, $c = 23.11$ Å, consistent with the experimental values ($a = b = 4.276$ Å, $c = 23.78$ Å) [34]. Its structure can be visualized in terms of a cubic-close-packed array of Te atoms, with Na and Cu occupying alternatingly the interstitial layers. Na is in an octahedral coordination with an average Na-Te bond length of 3.11 Å, and a small shift occurs for Na from the center of octahedral site towards the Te_2 atom. Cu atoms occupy the tetrahedral and octahedral voids with a small displacement from the centers of these sites. Cu_1 and Cu_2 are in tetrahedral coordination with an average Cu-Te bond length of 2.717 Å and 2.736 Å respectively. Cu_3 is in octahedral coordination with a large shift towards Te_1 [29].

By calculating band structure in the entire BZ, as shown in Fig. 2(b), we can find that $NaCu_3Te_2$ is an ideal TDP semimetal with the desired s^*-p band inversion solely along the ΓZ
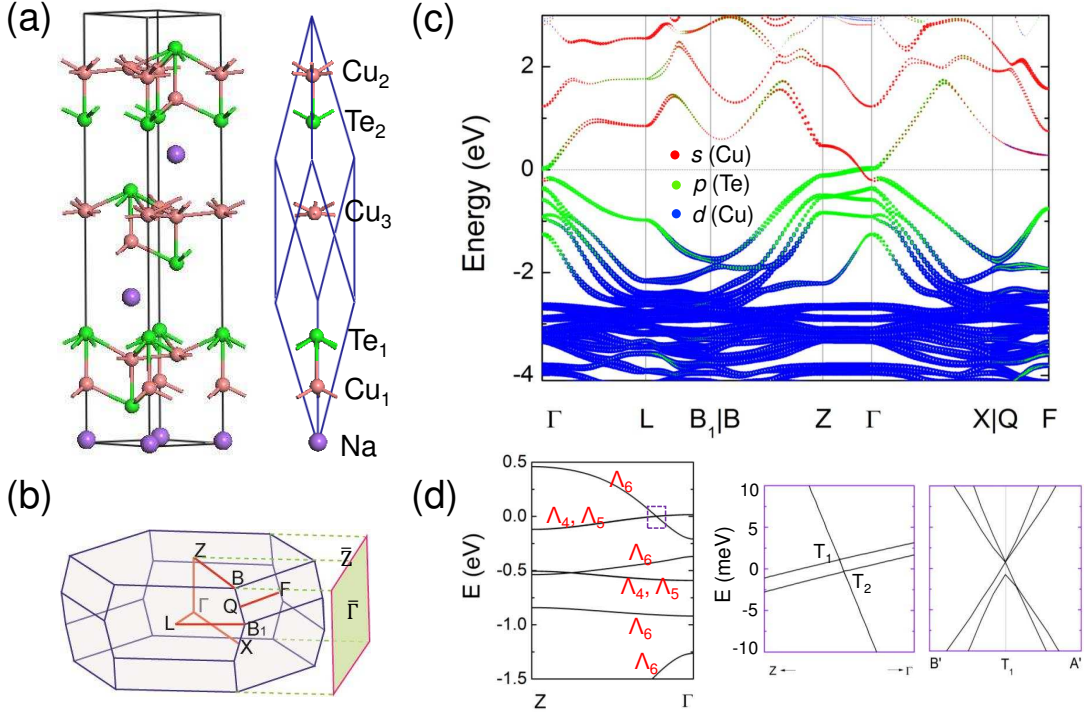
FIG. 2: (a) Conventional unit cell (black line) and primitive cell (blue line) of $NaCu_3Te_2$. In the primitive cell, two nonequivalent Te atoms are labeled as Te_1 and Te_2 while three nonequivalent Cu atoms are labeled as Cu_1, Cu_2 and Cu_3, respectively. (b) BZ of primitive cell of $NaCu_3Te_2$ and its projection towards (010) surface. The red lines in BZ depict the high-symmetry lines. (c) Band structure (with SOC effect) with different atomic orbitals projections. (d) Left panel: band structure along $Z\Gamma$ with the labels of three double-group representations. Middle and right panels: band structures around E_F along and perpendicular to the $Z\Gamma$ direction, respectively. Two TDPs are labeled by T_1 and T_2 points.

line that has the C_{3v} symmetry, as shown in Fig. 2(c). Along the ΓZ line, the C_{3v} symmetry group has one 2D (Λ_6) and two 1D (Λ_4, Λ_5) double-group representations. Including SOC effect, the s^* band (Λ_6 representation) belongs to double-degenerate $J_z = \pm 1/2$ states, whereas the p band ($p_{x,y}$ here, Λ_4 and Λ_5 representations) splits into two nondegenerate $J_z = \pm 3/2$ states, as demonstrated in left panel of Fig. 2(d). Consequently, the band crossing near E_F generates a pair of TDPs along $Z\Gamma$, as shown in the middle panel of Fig. 2(d). Along the direction perpendicular to $Z\Gamma$ line, each TDP will split into three nondegenerate bands, as revealed in the right panel of Fig. 2(d). Thus, the TDPs are strictly protected

4

by the C_{3v} symmetry. As expected from Fig. 1(b), along the other ΓZ line there is another pair of identical TDPs. The position of these two pairs of TDP in the momentum space are $(0, 0, \pm 0.0943 \text{ Å}^{-1})$ and $(0, 0, \pm 0.0924 \text{ Å}^{-1})$, respectively. The topological nature of TDPs in NaCu$_3$Te$_2$ is further confirmed by calculating the Z_2 topological invariants, which are well-defined in both the $k_z = 0$ $(Z_2 = 1)$ and $k_z = \pi$ planes $(Z_2 = 0)$ [29].

To understand the origin of TDPs, we start from the atomic energy levels and consider the effects of orbital hybridization, crystal-field splitting, and SOC on the band evolution in the vicinity of Γ point, as shown in Fig. 3(a). Without hybridizations, the Cu s, Te p and Cu d orbitals are close in energy. With hybridizations and crystal field splitting (stage I), the antibonding s^* and bonding p bands are formed, and the crystal-field effect makes the p_z orbital split from the double-degenerated $p_{x,y}$ orbitals. The additional strong p-d hybridizations upshift (downshift) the p (d) orbitals to higher (lower) energy positions. Among Te$_1$ and Te$_2$ atoms, the Te$_2$ atom has a stronger p-d hybridization effect due to the shorter Te$_2$-Cu bond lengths. Consequently, the Te$_2$ p orbitals will be pushed to higher energy levels [green solid lines in Fig. 3(a)] than that of Te$_1$ p orbitals [green dashed lines in Fig. 3(a)]. In the vicinity of Γ point, the Te$_2$ $p_{x,y}$ orbitals are pushed up to an even higher energy position than that of Cu s^* orbital, while at all other high-symmetry points all the Te p orbitals still have lower energies than that of Cu s^* orbital, which give rise to a band inversion solely around the Γ point in the entire BZ. In stage II, the SOC effect mixes spin and orbital angular momenta while preserving the total angular momentum. The $p_{x,y}$ orbitals further split into $J_z = \pm 3/2$ and $J_z = \pm 1/2$ states, meanwhile both s and p_z orbitals evolve into $J_z = \pm 1/2$ states. Around the Γ point, the (Te$_2$) $J_z = \pm 3/2$ states are still located above the s^*-type $J_z = \pm 1/2$ states. Along ΓZ, all $J_z = \pm 1/2$ states belong to the Λ_6 representation and $J_z = \pm 3/2$ states belong to the Λ_4 and Λ_5 representations. For the non-centrosymmetric system, the SOC effect can further lift the degeneracy of $J_z = \pm 3/2$ states, and as a result the band crossing of $J_z = \pm 3/2$ and $J_z = \pm 1/2$ states along ΓZ can generate two ideal TDPs in the whole BZ.

Since the energy splitting between the two TDPs along ΓZ in NaCu$_3$Te$_2$ is mostly contributed by the energy splitting of $J_z = \pm 3/2$ states, it is therefore crucial to develop understanding on what modulate the size of energy splitting between the $J_z = \pm 3/2$ (Λ_4 and Λ_5) states, which may be important for future applications. We discover that the splitting of Λ_4 and Λ_5 states is mostly contributed by the Dresselhaus SOC effect [42], which is proportional

to the momentum, $\Delta E = C_k k$, where k is along the direction with C_{3v} symmetry and C_k determines the size of splitting between the Λ_4 and Λ_5 states[29]. The C_k originates from the second-order interaction between the $J = 3/2$ states and the uppermost cation d core levels in the spin-orbit operator H_{so} [43]. It can be deduced $C_k = \alpha \Delta_d S \beta / [E(3/2) - E_d]$, where α is a constant, Δ_d is the spin-orbit splitting of the d orbitals of the cation with E_d of its energy, $E(3/2)$ is the valence band energy with $J = 3/2$ states, β is the admixture coefficient of d orbitals in the valence band, and S is the corresponding matrix element of momentum p $[S = i\langle 3/2|p_x|d_{x^2-y^2}\rangle]$. Therefore, the p-d hybridization, allowed only if the inversion symmetry is broken, together with spin-orbit splitting of d orbital of Cu, determines the splitting magnitude between Λ_4 and Λ_5 states in NaCu$_3$Te$_2$.

To confirm this, we have extended NaCu$_3$Te$_2$ to its family compounds AB_3X_2 ($A =$ Na, K; $B =$ Cu, Ag, Au; $X =$ S, Se, Te) by isovalent cation/anion replacements. These AB_3X_2 compounds could have similar stable structure to that of NaCu$_3$Te$_2$ according to our formation energy calculations [29]. Interestingly, some materials are intrinsic TDP semimetals while the others are semiconductors that need additional charge doping to shift the E_F to TDPs [29]. In all the AB_3X_2 compounds, the bands along ΓZ have similar characteristics as that of NaCu$_3$Te$_2$, i.e., the $p_{x,y}$ orbitals split into double-degenerate $J_z = \pm 1/2$ states and two nondegenerate $J_z = \pm 3/2$ states with SOC effect, and the splitting magnitude between these two $J_z = \pm 3/2$ states is determined by C_k. In Fig. 3(b), we have classified the maximum splitting energy (ΔE_m) between $J_z = \pm 3/2$ states in AB_3X_2 materials into three sub-groups in terms of the SOC strength of cation B (Cu, Ag, Au). Each sub-group has six materials, i.e., NaB_3X_2 ($X =$ S, Se, Te) and KB_3X_2 ($X =$ S, Se, Te). Generally, our calculations confirm that the SOC strength of B element will overall determine the maximal splitting of $J_z = \pm 3/2$, while the zero-order SOC of X anion has almost no impact on the energy splitting. Interestingly, in each sub-group the diversity of ΔE_m of AB_3X_2 ($A =$ Na, K; $X =$ S, Se, Te) as a function of A and X is contributed by the distinct p-d hybridization strength, i.e., the stronger the p-d hybridization, the larger the splitting between $J_z = \pm 3/2$ [29]. Another way to tune the p-d hybridization strength is strain (pressure) engineering. For example, we find that compressive (tensile) strain can increase (decrease) ΔE_m by increase (decrease) p-d hybridization [29]. Thus, our calculations not only verify our model, but also provide an effective way to modulate the energy splitting of $J_z = \pm 3/2$ states. It is also noted that the size of ΔE_m is not guaranteed to be the
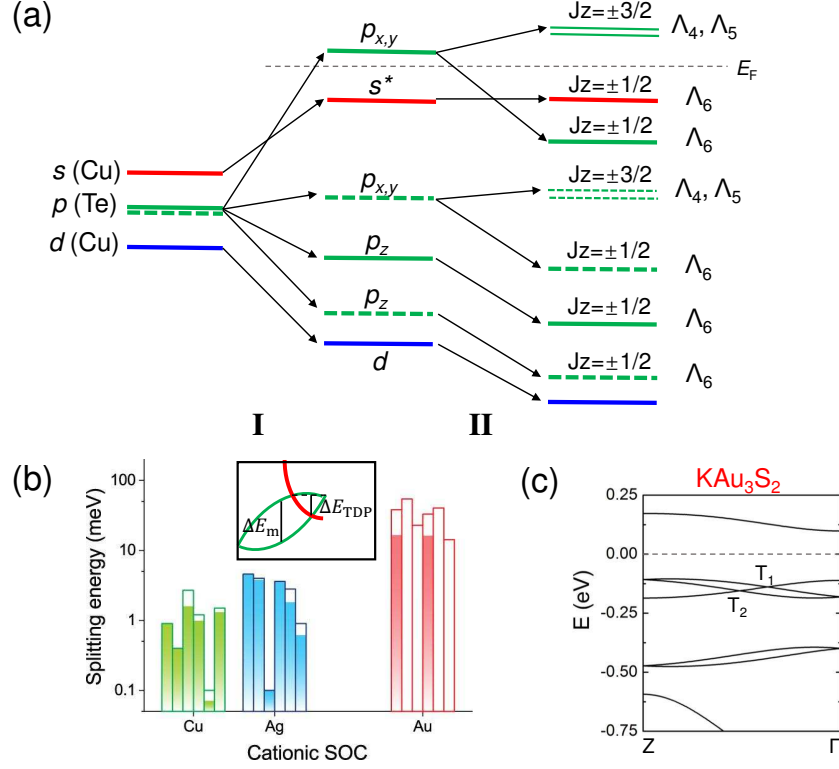
6

FIG. 3: (a) Schematic diagram of band evolution in the vicinity of Γ point: stage I represents the orbital hybridization and crystal-field splitting effect, and stage II represents SOC effect (see text). (b) The maximum splitting energy (ΔE_{m}) between two $J_z = \pm 3/2$ states (total column height) and the realistic splitting energy (ΔE_{TDP}) between two TDPs (solid column height) for AB_3X_2. ΔE_{m} and ΔE_{TDP} are illustrated in the inset, where band crossing occurs between $J_z = \pm 1/2$ (red) and $J_z = \pm 3/2$ (green) states. The $NaCu_3Te_2$ family are divided into three groups as $B = $ Cu, Ag, Au. For each group, six columns represent NaB_3X_2 ($X = $ S, Se, Te) and KB_3X_2 ($X = $ S, Se, Te) from left to right in sequence. (c) Band structure of KAu_3S_2 along $Z\Gamma$. The E_{F} is set to zero.

realistic energy splitting of two TDPs (ΔE_{TDP}), as the latter also depends on the position of band crossing between the $J_z = \pm 3/2$ and $J_z = \pm 1/2$ states, i.e., ΔE_{TDP} can be smaller than ΔE_{m}, as shown in Fig. 3(b). Generally, by the choices of specific AB_3X_2, ΔE_{TDP} can be dramatically tuned from several meV (such as $NaCu_3Te_2$) to dozens of meV [such as KAu_3S_2 in Fig. 3(c)].

$NaCu_3Te_2$ family can serve as ideal platforms to study the unique surface states and Fermi arcs of TDP semimetals. Fig. 4(a) shows the surface projected band for the (010) surface

of a semi-infinite $NaCu_3Te_2$ system. There is a clear Dirac cone-like surface state centering at $\bar{\Gamma}$ with upper (lower) branch connected to the conduction (valence) band. Along $\bar{\Gamma}\bar{X}$, the number of crossings between surface states and any in-gap energy level is odd, confirming the nontrivial Z_2 in the $k_z = 0$ plane. Along $\bar{\Gamma}\bar{Z}$, the two branches of topological surface states terminate at two bulk TDPs respectively. For the Fermi surfaces of $NaCu_3Te_2$ at different E_F [Fig. 4(b)]: When E_F ($E_F = 1$ meV) crosses one TDP (T_1), two pieces of Fermi arcs appear around $\bar{\Gamma}$ and they touch at the projection of T_1; When E_F ($E_F = -2$ meV) crosses the other TDP (T_2), another branch of Fermi arc appears and merges into the valence band; When E_F is further shifted to $E_F = -10$ meV, two branches of Fermi arcs coexist and they are separated along the high-symmetry line, which is related to the splitting of two adjacent TDPs.
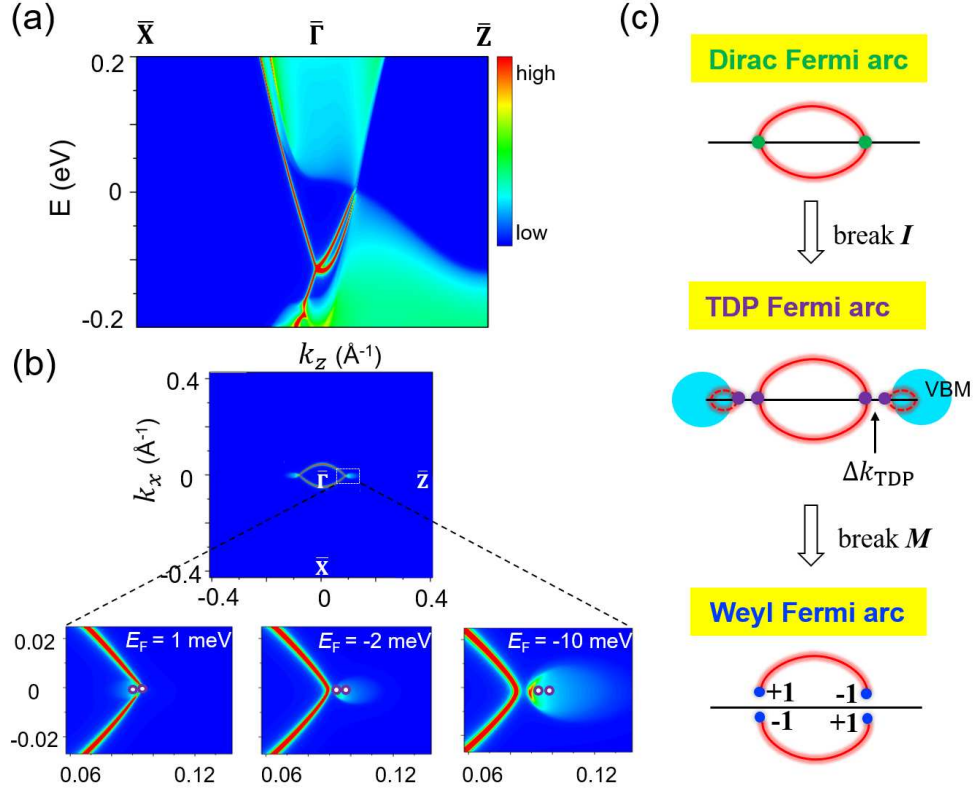

FIG. 4: (a) Surface projected band and (b) Fermi surfaces with different E_F for the (010) surface of a semi-infinite $NaCu_3Te_2$ system. Two circles in magnified Fermi surfaces denote the surface projections of two adjacent TDPs. (c) Evolution of Fermi arcs from Dirac to TDP to Weyl fermions (see text).

After obtain the ideal TDP Fermi arc, we can further understand the evolution of Fermi arcs from Dirac to TDP to Weyl fermions. For Dirac fermion, the two Fermi arcs touch at the projections of Dirac points, and they form a closed circle with a discontinuous Fermi velocity [Fig. 4(c), upper panel]. If the inversion symmetry ($\boldsymbol{I}$) of the system is broken but the C_{3v} symmetry is kept, each Dirac point can split into two adjacent TDPs along the high-symmetry line. Correspondingly, two branches of Fermi arcs are separated along this high-symmetry line [Fig. 4(c), middle panel]. The split of two TDPs (Δk_{TDP} or ΔE_{TDP}) will influence the separation of these two branches of Fermi arcs. If the mirror symmetry ($\boldsymbol{M}$) of the system is further broken, each TDP can further split into two Weyl points with opposite chirality. The split is moved away from the high-symmetry line, so that the Fermi arcs of Weyl points are disconnected [Fig. 4(c), bottom panel]. It is expected that the intrinsic characteristics of TDP fermions and the evolution of Fermi arc we discovered here can be experimentally confirmed in the future.

In conclusion, we disclose an effective approach to search for ideal TDP semimetals. We further discovered that the NaCu$_3$Te$_2$ family of compounds are ideal TDP semimetals with unique Fermi surface states and Fermi arcs. We also find an important mechanism to modulate the energy splitting between the two adjacent TDP nodes in these materials.

[1] M. Z. Hasan and C. L. Kane, Rev. Mod. Phys. **82**, 3045 (2010).

[2] X.-L. Qi and S.-C. Zhang, Rev. Mod. Phys. **83**, 1057 (2011).

[3] H. Weng, X. Dai, and Z. Fang, J. Phys.: Condens. Matter **28**, 303001 (2016).

[4] C.-K. Chiu, J. C. Y. Teo, A. P. Schnyder, and S. Ryu, Rev. Mod. Phys. **88**, 035005 (2016).

[5] A. Bansil, H. Lin, and T. Das, Rev. Mod. Phys. **88**, 021004 (2016).

[6] N. P. Armitage, E. J. Mele, and A. Vishwanath, arXiv:1705.01111.

[7] B. Q. Lv, H. M. Weng, B. B. Fu, X. P. Wang, H. Miao, J. Ma, P. Richard, X. C. Huang, L. X. Zhao, G. F. Chen, Z. Fang, X. Dai, T. Qian, and H. Ding, Phys. Rev. X **5**, 031013 (2015).

[8] S.-Y. Xu, I. Belopolski, N. Alidoust, M. Neupane, G. Bian, C. Zhang, R. Sankar, G. Chang, Z. Yuan, C.-C. Lee, S.-M. Huang, H. Zheng, J. Ma, D. S. Sanchez, B. Wang, A. Bansil, F. Chou, P. P. Shibayev, H. Lin, S. Jia, and M. Z. Hasan, Science **349**, 613 (2015).

[9] Z. K. Liu, B. Zhou, Y. Zhang, Z. J. Wang, H. M. Weng, D. Prabhakaran, S.-K. Mo, Z. X. Shen, Z. Fang, X. Dai, Z. Hussain, and Y. L. Chen, Science **343**, 864 (2014).

[10] S. Xu, C. Liu, S. K. Kushwaha, R. Sankar, J. W. Krizan, I. Belopolski, M. Neupane, G. Bian, N. Alidoust, T. R. Chang, H. T. Jeng, C. Y. Huang, W. F. Tsai, H. Lin, P. P. Shibayev, F. C. Chou, R. J. Cava, and M. Z. Hasan, Science **347**, 294 (2015).

[11] A. A. Soluyanov, D. Gresch, Z. Wang, Q. Wu, M. Troyer, X. Dai, and B. A. Bernevig, Nature **527**, 495 (2015).

[12] B. Bradlyn, J. Cano, Z. Wang, M. G. Vergniory, C. Felser, R. J. Cava, and B. A. Bernevig, Science **353**, aaf5037 (2016).

[13] S. Zaheer, S. M. Young, D. Cellucci, J. C. Y. Teo, C. L. Kane, E. J. Mele, and A. M. Rappe, Phys. Rev. B **87**, 045202 (2013).

[14] G. W. Winkler, Q. Wu, M. Troyer, P. Krogstrup, and A. A. Soluyanov, Phys. Rev. Lett. **117**, 076403 (2016).

[15] Z. Zhu, G. W. Winkler, Q. Wu, J. Li, and A. A. Soluyanov, Phys. Rev. X **6**, 031003 (2016).

[16] H. Weng, C. Fang, Z. Fang, and X. Dai, Phys. Rev. B **93**, 241202 (2016).

[17] H. Weng, C. Fang, Z. Fang, and X. Dai, Phys. Rev. B **94**, 165201 (2016).

[18] G. Chang, S.-Y. Xu, S.-M. Huang, D. S. Sanchez, C.-H. Hsu, G. Bian, Z.-M. Yu, I. Belopolski, N. Alidoust, H. Zheng, T.-R. Chang, H.-T. Jeng, S. A. Yang, T. Neupert, H. Lin, and M. Z. Hasan, Sci. Rep. **7**, 1688 (2017).

[19] X. Zhang, Z.-M. Yu, X.-L. Sheng, H. Y. Yang, and S. A. Yang, Phys. Rev. B **95**, 235116 (2017).

[20] J. Yu, B. Yan, and C.-X. Liu, Phys. Rev. B **95**, 235158 (2017).

[21] H. Yang, J. Yu, S. S. P. Parkin, C. Felser, C.-X. Liu, and B. Yan, arXiv:1706.00200.

[22] J. B. He, D. Chen, W. L. Zhu, S. Zhang, L. X. Zhao, Z. A. Ren, and G. F. Chen, Phys. Rev. B **95**, 195165 (2017).

[23] Y. Xu and L.-M. Duan, arXiv:1705.05780.

[24] B. Q. Lv, Z.-L. Feng, Q.-N. Xu, X. Gao, J.-Z. Ma, L.-Y. Kong, P. Richard, Y.-B. Huang, V. N. Strocov, C. Fang, H.-M. Weng, Y.-G. Shi, T. Qian, and H. Ding, Nature (2017)

DOI:10.1038/nature22390.

[25] C. Shekhar, Y. Sun, N. Kumar, M. Nicklas, K. Manna, V. Suess, O. Young, I. Leermakers, T. Foerster, M. Schmidt, L. Muechler, P. Werner, W. Schnelle, U. Zeitler, B. Yan, S. S. P. Parkin, and C. Felser, arXiv:1703.03736.

[26] J.-Z. Ma, J.-B. He, Y.-F. Xu, B.-Q. Lv, D. Chen, W.-L. Zhu, S. Zhang, L.-Y. Kong, X. Gao, L.-Y. Rong, Y.-B. Huang, P. Richard, C.-Y. Xi, Y. Shao, Y.-L. Wang, H.-J. Gao, X. Dai, C. Fang, H.-M. Weng, G.-F. Chen, T. Qian, and H. Ding, arXiv:1706.02664.

[27] W. A. Harrison, *Electronic Structure and Properties of Solids* (Freeman, San Francisco, 1980).

[28] S.-H. Wei and A. Zunger, Phys. Rev. Lett. **59**, 144 (1987).

[29] See Supplemental Material for details of computational methods, crystal structure, band structure without SOC, calculation of Z_2 topological invariants, the splitting of Λ_4 and Λ_5 states with k, formation energies and band structures of $NaCu_3Te_2$ family of materials, and strain effect on ΔE_{m}, which also includes Refs. [30–41].

[30] G. Kresse and J. Furthmüller, Comput. Mater. Sci. **6**, 15 (1996).

[31] G. Kresse and J. Furthmüller, Phys. Rev. B **54**, 11169 (1996).

[32] P. E. Blöchl, Phys. Rev. B **50**, 17953 (1994).

[33] J. P. Perdew, K. Burke, and M. Ernzerhof, Phys. Rev. Lett. **77**, 3865 (1996).

[34] K. O. Klepp, Z. Naturforsch. B **42**, 130-134 (1987).

[35] S. Grimme, J. Antony, S. Ehrlich, and S. Krieg, J. Chem. Phys. **132**, 154104 (2010).

[36] N. Marzari and D. Vanderbilt, Phys. Rev. B **56**, 12847 (1997).

[37] I. Souza, N. Marzari, and D. Vanderbilt, Phys. Rev. B **65**, 035109 (2001).

[38] M. P. L. Sancho, J. M. L. Sancho, and J. Rubio, J. Phys. F **14**, 1205 (1984).

[39] M. P. L. Sancho, J. M. L. Sancho, J. M. L. Sancho, and J. Rubio, J. Phys. F **15**, 851 (1985).

[40] R. Yu, X. L. Qi, A. Bernevig, Z. Fang, and X. Dai, Phys. Rev. B **84**, 075119 (2011).

[41] A. A. Soluyanov and D. Vanderbilt, Phys. Rev. B **83**, 235401 (2011).

[42] G. Dresselhaus, Phys. Rev. **100**, 580 (1955).

[43] M. Cardona, N. E. Christensen, and G. Fasol, Phys. Rev. Lett. **56**, 2831 (1986).